nesco

19 May 1967

S-424

FEASIBILITY ANALYSIS OF PARACHUTE ENTRY FOR MARS LANDER

NATIONAL ENGINEERING SCIENCE CO.

SUBSIDIARY OF PIKE CORPORATION OF AMERICA

711 SOUTH FAIR OAKS AVENUE, PASADENA, CALIFORNIA 91105
1875 CONNECTICUT AVE., N.W., WASHINGTON, D.C.

FEASIBILITY ANALYSIS OF PARACHUTE ENTRY FOR MARS LANDER

Report No. S-424

Prepared for

Jet Propulsion Laboratory
4800 Oak Grove Drive
Pasadena, California

Prepared by

E. Mayer, Ph.D

P.O. EC-437910

This work was performed for the Jet Propulsion Laboratory, California Institute of Technology, sponsored by the National Aeronautics and Space Administration under Contract NAS7-100.

NATIONAL ENGINEERING SCIENCE COMPANY
711 South Fair Oaks Avenue
Pasadena, California 91105

19 May 1967

CONTENTS

CONTENTS
(Continued)

NOMENCLATURE

Most of the symbols listed here are more fully defined in the text. Unless otherwise indicated in the text, the symbols have the units listed here:

Symbols		Units
C_D	drag coefficient	--
c_e	ballistic entry parameter	ft^3/lb
D	diameter of canopy, length of shroud line	ft
f	breaking tenacity of fabric	gm/denier
g	gravity acceleration	ft/sec^2
H	atmospheric density scale height	ft
J	mechanical equivalent of heat	ft-lb/BTU
N_s	number of shroud lines	--
p_{max}	maximum dynamic pressure	lb/ft^2
R	radius	ft
Q	heat flux	BTU/ft^2sec
T	absolute temperature	deg R
V	velocity	ft/sec
$\lvert\dot{V}\rvert$	deceleration	ft/sec^2
W	weight	lb
x	coordinate along symmetry axis	ft
y	coordinate normal to symmetry axis	ft
z	altitude	ft
z_{max}	altitude of peak dynamic pressure	ft

α	angle between incident Newtonian flow and surface normal	radian
β	ballistic coefficient	$slugs/ft^2$
γ	angle between velocity vector and local horizontal	radian
δ	effective thickness of canopy	ft
ϵ	gray-body emissivity	--
λ	molecular mean free path	ft
λ_o	molecular mean free path in air at sea level	ft
μ	fractional weight	--
ρ	density	lb/ft^3
ρ_o	density of air at sea level	lb/ft^3
ρ_E	density parameter of Earth atmosphere	lb/ft^3
ρ_M	density parameter of Mars atmosphere	lb/ft^3
σ	stress	lb/ft^2
σ'	Stefan-Boltzmann constant	$BTU/ft^2 sec\ deg^4 R$

Subscripts

a	axial
bl	boundary layer
c	canopy
e	entry
E	Earth
fm	free molecule flow
h	hoop

M	Mars
max	maximum
min	minimum
r	ring
s	shroud
tr	transitional flow

The abbreviation log refers to natural logarithm.

1. SUMMARY

The feasibility of a parachute entry system for a Mars lander has been investigated in accordance with a work statement appended to this report. The principal restrictions in the work statement specify the range of ballistic coefficients $10^{-1} \geq \beta$ slugs/ft^2 $\geq 10^{-3}$, the weight of the deceleration system limited to not more than payload weight $W_p = 50$ lb, entry velocities in the range $6 \leq V_e$ kft/sec ≤ 16. Furthermore, consideration of a high-temperature high-strength plastic (Nomex) undergoing "laminar" peak heating is specified in the work statement.

It was found that with the above restrictions, feasibility limit conditions are reached for entry velocity $V_e = 6.3$ kft/sec in a parachute system with ballistic coefficient $\beta \simeq 2 \times 10^{-2}$ slugs/ft^2. At this feasibility limit most of the system weight is needed to provide a "massive" blunted leading edge for canopy, so as to alleviate the laminar heat transfer, and thereby prevent the development of temperature in excess of the permissible maximum for Nomex, $T_{max} \simeq 500^{\circ}$F, at the leading edge.

It was found, further, that greater entry speeds are feasible if the restriction to "laminar" peak heat transfer is relaxed and design configurations with sharp leading or windward elements are taken into consideration. Therefore, additional configurations with peak heating in the free molecule flow and/or transitional flow regimes have been also analyzed in a first approximation. In these configurations the principal design parameters, canopy leading edge radius R_r and shroud line cross sectional radius R_s are constrained by two conflicting requirements: (1) they must be sufficiently small to assure the occurrence of peak heat flux in the free molecule flow regime and (2) they must be sufficiently large to provide structural strength against the peak deceleration loads.

Both requirements can be satisfied with all-Nomex parachutes over the range of β considered here. Furthermore, at the lowest value $\beta = 10^{-3}$, the feasible maximum entry velocity is $V_e = 9.7$ kft/sec, a significant increase over that found for the laminar heating pulse. The $\beta = 10^{-3}$ configuration is feasible, for example, with the following design dimensions; canopy thickness δ and leading edge radius R_r equal to about .001 in; shroud line radius $R_s = .0036$ in, number of shroud lines $N_s = 300$; diameter of canopy, taken equal to the length of the shroud lines, is $D = 76.5$ ft. The corresponding canopy weight $W_c = 23.3$ lb and shroud weight $W_s = 0.6$ lb total less than half of the maximum chute weight of 50 lb under consideration. It is to be noted that, for $\beta = 10^{-3}$, the theoretically feasible minimum dimensions δ, R_s, etc., adequate for peak dynamic load, require a minimum Nomex parachute weight of about 1 lb.

The low-weight requirements of the design examples summarized suggest that, by utilizing high-temperature, high-strength metals for parachutes, having the sharp windward edge dimensions to assure peak heat load in free molecule flow, the feasible entry velocities may be significantly increased without exceeding the system weight limitation of 50 lb. The possible extension of the velocity limit without exceeding the weight limit is illustrated in the following table which compares Nomex ($T_{max} = 500^{\circ}F$) performance with that of steel ($T_{max} = 1000^{\circ}F$).

Maximum V_e with Heating Pulse in Free Molecule Flow

β slugs/ft^2	10^{-1}	10^{-2}	10^{-3}
V_e ft/sec (Nomex at 500°F)	2090	4510	9700
V_e ft/sec (Steel at 1000°F)	3660	7890	17,000

2. INTRODUCTION

This report presents the results of an analytic investigation performed by National Engineering Science Company (NESCO) under Jet Propulsion Laboratory Purchase Order No. EC437910. The contract task requirements are specified in a work statement included here in the Appendix. As indicated in the work statement, the objective of the investigation is to perform a first order parametric analysis which defines the feasibility limits of a Mars entry capsule decelerated by an annular parachute.

The assumptions employed are summarized in Section 3. These assumptions serve to define, in the first place, the general configuration of the entry system, and the structural elements which are subjected to critical peak dynamic and heat loads during entry. Furthermore, the assumptions specify the simplified deceleration and heat transfer laws employed in the analysis, consistent with the scope of the first order analysis. Justification of these assumptions is detailed in the text where the development of the simplified entry equations is presented.

Starting with the second order shallow entry equations, a description of the trajectory is obtained in Section 4 expressing the relation between speed V and altitude z in an elementary form convenient for the analysis of peak dynamic loads and heat loads. The critical stress formulas associated with peak deceleration loads are given in Section 5. The peak heat loads are determined in Section 6 for the various regimes of free molecule flow, transitional and continuum flow encountered in descent through the Mars atmosphere. The feasibility limits, illustrated for Nomex in particular, are determined in Section 7, by expressing the peak temperature as function of entry velocity for a range of ballistic coefficients and deceleration system weights under consideration. The results are discussed in Section 8, followed by remarks on shock impingements in Section 9.

The salient conclusions, responsive to the work statement in the Appendix, are summarized in Section 10.

3. BASIC ASSUMPTIONS

3.1 Configuration and Major System Components

The usual definition of the ballistic coefficient

$$\beta = \frac{W/g_E}{C_D A} \tag{3.1}$$

may be converted into the following expression for calculating the range of diameters D of interest in this investigation:

$$D = \sqrt{\frac{4A}{\pi}} = \sqrt{\frac{8\,(W/g_E)}{\pi\beta}} \tag{3.2}$$

where $C_D = 1/2$ has been substituted. Since W may vary over the range

$$50 \text{ lbs} = W_p < W \lesssim 2W_p = 100 \text{ lbs} \tag{3.3}$$

and β ranges from 10^{-3} to 10^{-1} slugs/ft^2, we obtain the following extreme values of D :

$$D_{min} = \sqrt{\frac{8}{\pi}\,\frac{(50/32.2)}{10^{-1}}} = 6.3 \text{ ft}$$

$$D_{max} = \sqrt{\frac{8}{\pi}\,\frac{(100/32.2)}{10^{-3}}} = 89 \text{ ft} \tag{3.4}$$

In view of the relatively large diameters $D \lesssim D_{max}$ available for low-β entry systems, the drag on the conical canopy is generally incurred under continuum flow conditions even at extreme altitudes in the low-density Martian atmosphere. Accordingly, by considering that the

coefficient $C_D = 1/2$ is associated with Newtonian continuum drag, it is inferred that the angle α between the incident axisymmetric wind and the canopy surface is $\alpha = 45^o$.

Three major components are envisaged in the configuration of the deceleration system: (a) shroud lines of length D , attached to the (b) conical canopy extending between the leading diameter D and trailing diameter $D' = D/\sqrt{2}$, in view of the given projected canopy area of $\frac{1}{2}(\frac{\pi}{4}D^2)$, and (c) a structural ring or torus of diameter D , with cross sectional radius R_r , for attachment of the shroud lines to the canopy. A sketch of the system is shown in Fig. 1.

As we shall see from heat transfer considerations, it may be desirable to reduce the cross sectional radius R_r to a minimum value, in order to realize free molecule flow heat transfer at the higher altitudes where peak heat loads develop. Thus, if direct attachment of the shroud lines to the canopy can be achieved, the torus may be altogether absent, leaving the leading edge of the canopy relatively sharp, with cross sectional radius comparable with the canopy thickness. The feasibility limit of entry at higher velocities V_e is crucially dependent on the possibility of realizing low-β systems with direct attachment of fine shroud lines to a thin canopy.

3.2 Trajectory Equations

The entry trajectory is described by the so-called second order solution (Ref. 2) in the approximation of small variations of the velocity vector relative to the local horizontal. In this approximation we assume in effect that the velocity is dependent primarily on the local altitude in accordance with the Gazley formula for constant ballistic coefficient bodies descending in an exponential atmosphere.

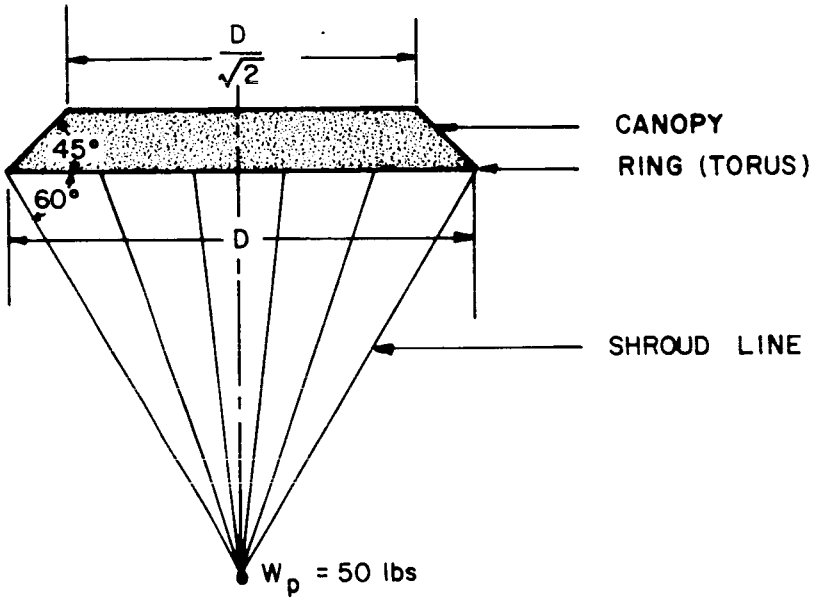

Figure 1

Sketch of annular parachute, showing general configuration

PA-2-10522

3.3 Dynamic Loads

It is assumed that the critical dynamic loads arise at the instant of maximum deceleration. The critical stresses of interest are those arising in (1) the leading edge of the canopy and (2) the shroud lines at their attachment to the canopy.

3.4 Heat Transfer

In regard to heat transfer in the free molecule flow regime, it is assumed that all surfaces have an accommodation factor of unity and that molecular impact is followed by diffuse reflection.

In regard to continuum heat transfer, it is assumed that stagnation heat transfer formulas based on air data can be applied to the Mars atmosphere.

A special interpolation formula between free molecule and stagnation heat transfer is postulated for transitional flow heat transfer.

3.5 Maximum Temperature

It is assumed that maximum temperatures are attained under quasi-equilibrium between aerodynamic heat influx and gray-body thermal re-radiation. Uniform local temperatures are assumed to prevail throughout any cross section of the shroud lines or of the canopy leading edge (ring or torus). Gray-body emissivities close to unity are assumed in numerical applications.

4. SIMPLIFIED TRAJECTORY EQUATIONS

The second order solution (Ref. 2) pertinent to small angles of inclination γ_e is employed in the calculation of entry trajectories. For exponential density variation of the type

$$\rho = \rho_M e^{-z/H_M} \tag{4.1}$$

the velocity V and inclination γ are interrelated by

$$V = V_e \exp - c_e \left[\frac{(\gamma - \gamma_e) \sin \gamma_e}{\cos \gamma_e - \cos \gamma}\right] (\rho - \rho_e) \tag{4.2}$$

$$\cos \gamma = \frac{\cos \gamma_e}{1 + \frac{H_M}{R_M}\left(\frac{g_M R_M}{V^2} - 1\right)\left(1 - \frac{\rho_e}{\rho}\right)} \tag{4.3}$$

where

$$c_e = \frac{H_M}{2\beta \sin \gamma_e} \tag{4.4}$$

The parameters of the exponential atmosphere introduced in Eq. (4.1) are determined from density data shown in Fig. 2 for the VM-3 and VM-7 engineering models. The VM-3 model data shown in Fig. 2 for the z range exceeding 200 kft is based on trajectory computer data furnished by JPL.* The VM-7 density is about one-half that of the VM-3 in the altitude range shown.

---

* JPL Trajectory Data Run 109 for R. Weaver, 8/27/66, communicated by E. Laumann.

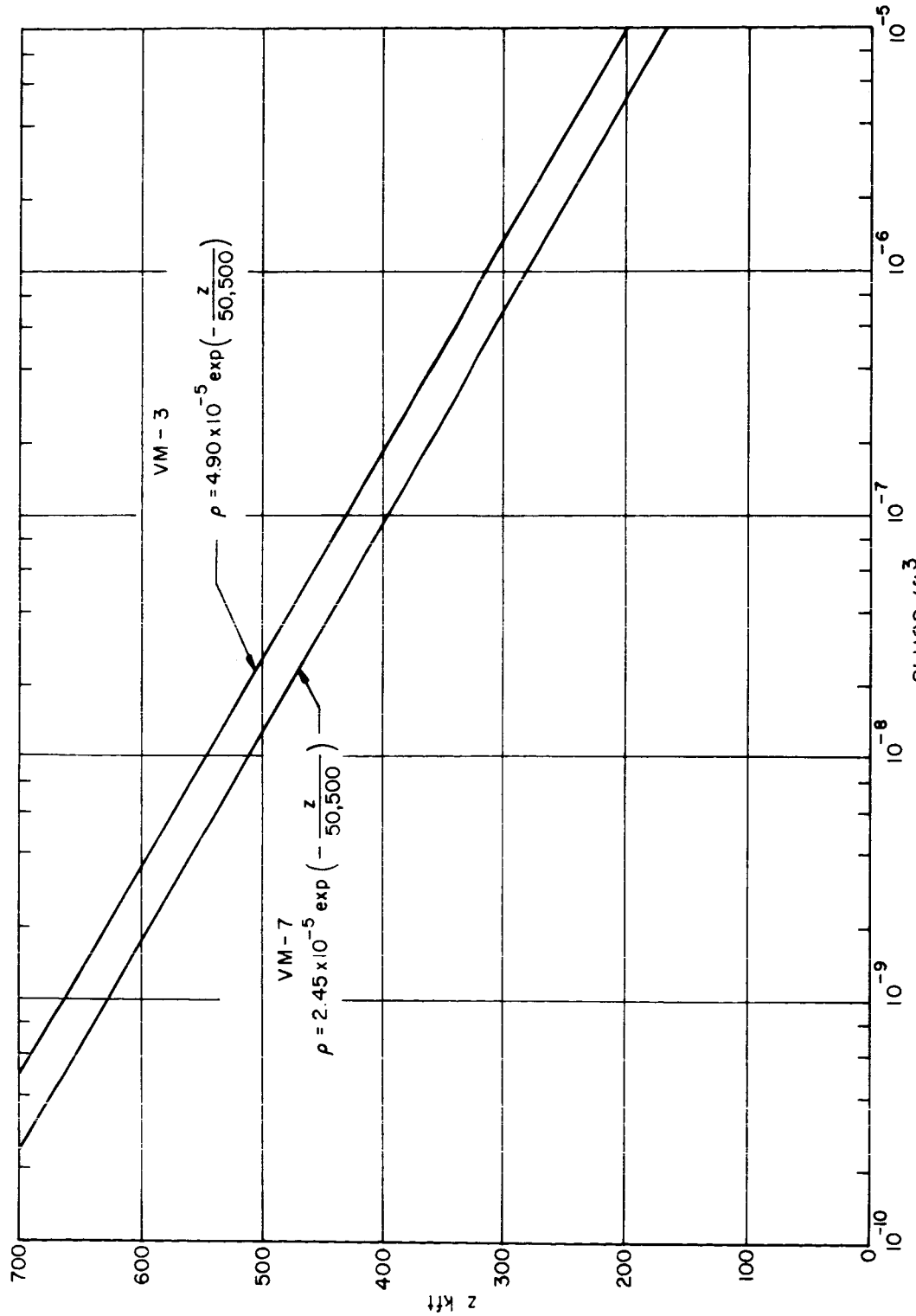

Figure 2

High altitude atmospheric density on Mars (VM-3, VM-7 models)

PA-3-10523

Table of Mars Atmosphere Parameters

Parameter	H_M kft	$10^5 \rho_M$ slugs/ft^{-3}
VM-3	50.5	4.90
VM-7	50.5	2.45

It is interesting to note that, notwithstanding the low surface density parameter ρ_M compared with that on earth, $\rho_E = 3.4 \times 10^{-3}$ slugs/ft^3 (Ref. 1, p. 13), the high altitude Mars atmosphere is favorable to deceleration effects owing to the larger Mars scale $H_M > H_E = 22$ kft. The data on the above table, in fact, imply that the Mars density exceeds that of the earth at altitudes above 165 kft for the VM-3 and 192 kft for the VM-7 models, respectively.

Considerable simplifications are effected in Eqs. (4-2, 4-3) by noting from Eq. (4.3) that under representative entry conditions of interest, the variation of $\cos\gamma$ in the high altitude trajectory is small down to the levels of peak heating and peak deceleration. This is readily seen by considering Mars data

$g_M = 12.3$ ft/sec^2 $\quad R_M = 2120$ mi $\quad \sqrt{2g_M R_M}$ (esc. vel.) $= 1.66 \cdot 10^4$ ft/sec

and decelerated speeds* $V \sim \frac{1}{2} V_e \sim 3000$ ft/sec , well below the critical stress and heat loading conditions of interest. For the preceding data Eq. (4.3) yields

* The lowest entry speed of interest $V_e = 6000$ ft/sec is employed here, since for larger V_e, the inclination γ differs from γ_e by less than the extreme difference shown in Eq. (4.5).

$$\cos\gamma = \frac{\cos\gamma_e}{1 + \frac{9.55}{2120}\left(\frac{(1.17)^2}{.3^2} - 1\right)} \simeq 0.94\cos\gamma_e \qquad (4.5)$$

We therefore find that for the shallow entry angle $\gamma_e = 15^\circ$ the bracketed quantity in Eq. (4.2) is very close to unity in the altitude and speed regime of interest. Thus, we find from Eq. (4.5)

$$.92 \leq \frac{(\gamma - \gamma_e)\sin\gamma_e}{\cos\gamma_e - \cos\gamma} \leq 1 \qquad (4.6)$$

In view of the preceding relation, the velocity equation (4.2) reduces to the familiar expression obtained by Gazley (Ref. 3) for steep reentry:

$$V = V_e \exp - c_e \rho \qquad (4.2')$$

where we have set $\rho_e << \rho$ in the deceleration regime of interest. We shall employ Eq. (4.2') in the calculation of peak stresses and heat loads which, as has been shown, depend primarily on the altitude z implicit in ρ and only weakly on the local inclination γ. For accuracy in trajectory calculations, beyond the scope of the present study, both z and γ would have to be determined by simultaneous solution of Eqs. (4.2) and (4.3).

A special consequence of the simplified trajectory in Eq. (4.2') is that the maximum deccleration, associated with maximum dynamic pressure $\rho V^2/2$, is independent of β [Cf. Eq. (3-20) of Ref. 1]:

$$\left|\dot{V}\right|_{max} = \left|\frac{dV}{dt}\right|_{max} = \frac{V_e^2 \sin\gamma_e}{2\,e\,H_M} \qquad (4.7)$$

However, the altitude $z = z_{max}$ at which the peak deceleration occurs depends on β as given by [Cf. Eq. (3-30) of Ref. 1]

$$z_{max} = H_M \log \frac{H_M \rho_M}{\beta \sin \gamma_e} \tag{4.8}$$

For example, for representative data of interest $V_e = 10^4$ ft/sec, $\sin \gamma_e = 0.259$, $\beta = 0.01$ slugs/ft^2, we find the peak deceleration of 92.0 ft/sec^2 occurring at the altitude 346 kft in the VM-3 and an altitude of 312 kft in the VM-7 atmosphere models.

We conclude this section by comparing the V versus z trajectory based on Eq. (4.2') with the JPL 6-degree of freedom trajectory result for $\beta = 10^{-2}$ at entry conditions $\gamma_e = 20^\circ$, $V_e = 13,190$ ft/sec, $z_e = 780$ kft. The agreement in the comparison shown in Fig. 3 is plausible, indicating that for the purpose of the present calculations the analytic results of this section will be sufficiently accurate. The analytic results provide, of course, the advantages of utmost simplicity in the calculation of maximum heat load and stress load during entry.

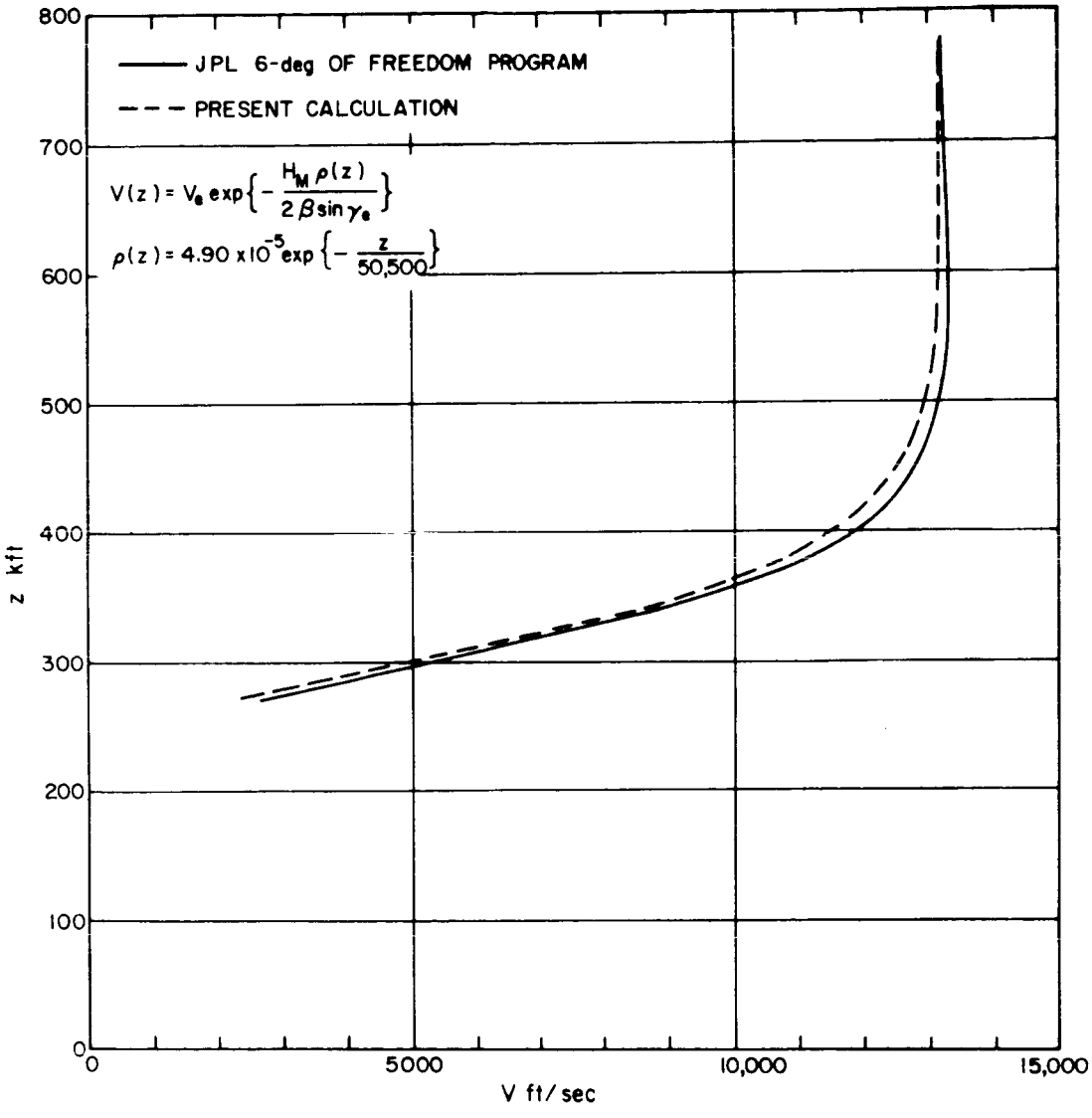

Figure 3

Comparison of calculated entry trajectories ($\beta = 10^{-2}$ slugs/ft^2, γ_e = 20 deg, z_e = 780 kft, V_e = 13.19 kft/sec, VM-3 atmosphere model)

PA-3-10524

5. MAXIMUM DECELERATION STRESSES

In this section we describe the maximum stresses associated with maximum deceleration loads on the entry system sketched in Fig. 1. In particular, we consider the hoop stress in the canopy and the axial stress in the shroud lines at maximum deceleration.

5.1 Hoop Stress in the Canopy

The maximum pressure on the canopy, calculated from Newtonian flow incident at the angle α with respect to the local surface normal:

$$p_{max} = (\rho V^2)_{max} \cos^2\alpha = 2\beta \left|\dot{V}\right|_{max} \cos^2\alpha \tag{5.1}$$

where $\left|\dot{V}\right|_{max}$ is given by Eq. (4.7). Therefore the hoop stress, in accordance with the standard formula for a conical shell of local diameter D, is

$$\sigma_h = \frac{p_{max}\, D}{2\delta \sin\alpha} = \frac{\beta \left|\dot{V}\right|_{max} D \cos^2\alpha}{\delta \sin\alpha} \tag{5.2}$$

where δ is the effective shell thickness and $\alpha = 45^\circ$ (see Fig. 1). We impose the requirement that σ_h shall not exceed the allowed stress σ_c of the canopy material

$$\sigma_h \leq \sigma_c \tag{5.3}$$

Consequently, in view of Eq. (5.2), δ must not be less than a minimum value

$$\delta \geq \delta_{min} = \beta \left|\dot{V}\right|_{max} D \cos^2\alpha \csc\alpha / \sigma_c \tag{5.4}$$

The tensile strength or breaking tenacity f of fabrics is usually expressed in units of gm/denier, which may be converted to σ_c in lbs/ft^2 by the conversion formula

$$\sigma_c = 2.95 \times 10^4 \, f \, \rho_c \tag{5.5}$$

where ρ_c is the material density in lbs/ft^3.

Density ρ_c and f data for the principal plastic under consideration here, Nomex, are shown in Fig. 4, obtained from Ref. 4. It is to be noted that the tensile strength σ_c at $500^\circ F$ obtained from this figure at $f = 3$ is $\sigma_c = 7.64 \times 10^6 \ lb/ft^2 = 53,000 \ lb/in^2$, roughly one-half that of stainless steel. Other high tenacity plastics, such as Dacron, indeed possess tensile strengths comparable with steel (Ref. 5). However, because of inferior high temperature properties, they will not be further considered here.

We illustrate the order of magnitude δ_{min} to show that the peak stress loads can be met with a relatively small effective Nomex thickness δ and, consequently, small canopy weight compared with payload weight. To express the dependence of δ_{min} on entry velocity V_e and ballistic coefficient β, we rewrite Eq. (5.4) replacing $\left|\dot{V}\right|_{max}$ from Eq. (4.7) and replacing D by use of the approximation [Cf. Eq. (3.2)]

$$D = \sqrt{\frac{8 \, W}{\pi \, g_E \, \beta}} \approx \sqrt{\frac{8 \, W_p}{\pi \, g_E \, \beta}} \tag{5.6}$$

The result is

$$\delta_{min} \simeq \frac{(V_e^2 \sin \gamma_e)}{2 \, e \, H_M \, \sigma_c} \sqrt{\frac{8 \, W_p \, \beta}{\pi \, g_E}} \cos^2 \alpha \csc \alpha \tag{5.7}$$

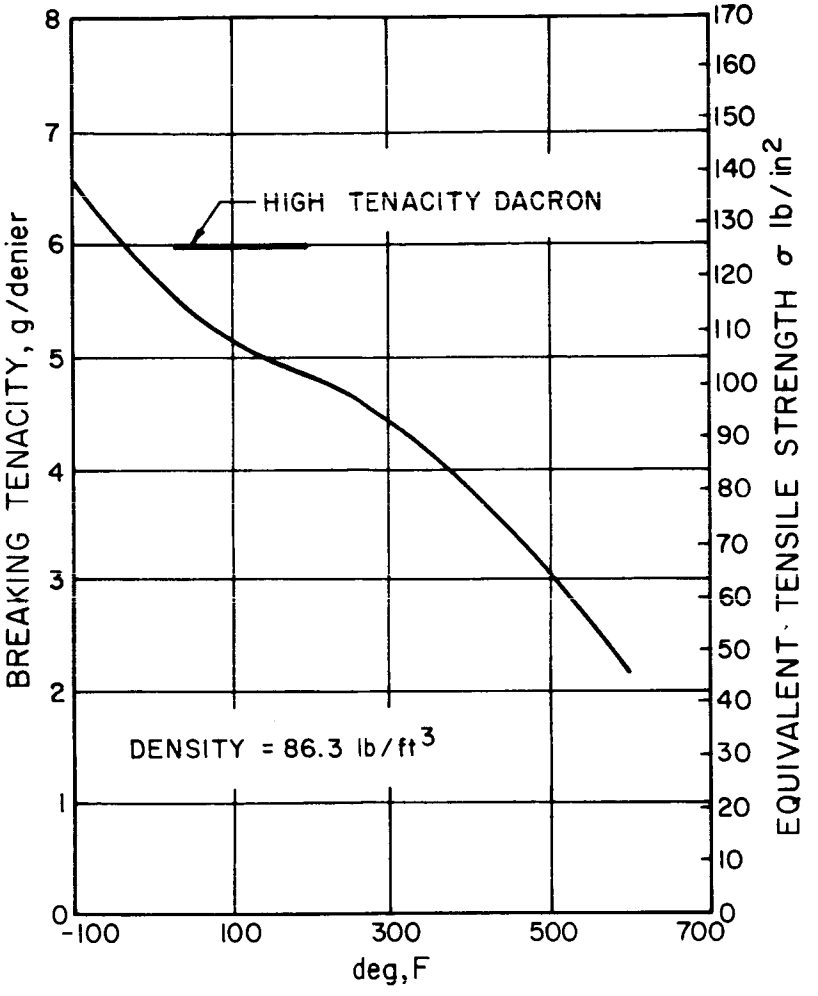

Figure 4

Breaking tenacity of NOMEX at various temperatures

PA-3-10525

Calculation from Eq. (5.7) with the Nomex datum $\sigma_c = 53,000$ lb/in^2 and $\alpha = 45^\circ$ indicates that even for the extreme values of $V_e = 16$ kft/sec, $\beta = 10^{-1}$

$$\delta_{min} \simeq 1.4 \times 10^{-5} \text{ ft} \tag{5.8}$$

The associated canopy weight is

$$W_{c,min} = \frac{\pi \delta_{min} D^2 \rho_c}{8 \cos \alpha} \simeq .0.027 \text{ lb} \tag{5.9}$$

which is indeed small compared with W_p. A much greater canopy weight would be required for the large diameter canopy with low β since W_c scales with β according to $W_c \sim \delta_{min} D^2 \sim \sqrt{\beta}\ \beta^{-1} \sim \beta^{-1/2}$. Thus for $\beta = 10^{-3}$ slugs/ft^2, the minimum canopy weight required for meeting the peak hoop load is 0.27 lb.

5.2 Axial Stress in Shroud Lines

The maximum axial stress σ_a in the shroud lines is associated with the maximum deceleration of the combined payload and shroud line masses $(W_p + W_s)/g_E$. For the assumed configuration in Fig. 1, the stress equation is

$$\frac{W_p + W_s}{g_E} \left| \frac{dV}{dt} \right|_{max} = A_s \sigma_a \sin 60^\circ = \pi R_s^2 N_s \sigma_a \sin 60^\circ \tag{5.10}$$

where the total cross sectional area A_s is the sum due to N_s shroud lines of radius R_s.

In the preceding formula the shroud design parameters N_s, R_s are also implicit in W_s, as given by

$$W_s = \pi R_s^2 N_s D \rho_s \tag{5.11}$$

Inasmuch as σ_a must not exceed the permissible stress level σ_s in the shroud material, Eq. (5.10) represents a limitation on the choice of the parameters N_s, R_s. For the decelerations $\left|dV/dt\right|_{max}$ obtained in Eq. (4.7) it is found that $\sigma_a \leq \sigma_s$ can be readily achieved with shroud weight $W_s << W_p$ and, therefore, to a high degree of approximation the choice of R_s, N_s is governed by the constraint

$$N_s R_s^2 \gtrsim \frac{W_p}{\pi g_E} \left|\frac{dV}{dt}\right|_{max} \frac{\csc 60^o}{\sigma_s} \tag{5.12}$$

To estimate the order of magnitude of $N_s R_s^2$, we rewrite Eq. (5.12) in the form

$$N_s R_s^2 \gtrsim \frac{1}{\pi} \frac{W_p}{g_E} \left(\frac{V_e^2 \sin \gamma_e}{2 e H_M}\right) \frac{\csc 60^o}{2.95 \times 10^4 f \rho_s} \tag{5.13}$$

and substitute Nomex data at $V_e = 16$ kft/sec as in Section 5.1. The result is

$$(N_s R_s^2)_{min} \simeq 1.9 \times 10^{-5} \text{ ft}^2 \tag{5.14}$$

The associated minimal shroud line weights in Eq. (5.11) range between $W_{s,min} = .032$ lb for $D_{min} = 6.3$ ft and $W_{s,min} = .46$ lb for $D_{max} = 89$ ft.

It is apparent from the results of this section that the weight restriction $W_s + W_c \lesssim W_p$ imposes no difficulty in designing to meet maximum dynamic stresses with the "fine-dimension" criteria of Eqs. (5.8, 5.14). Indeed the weight limitation will not be exceeded even with linear dimensions R, δ, ten times greater than those obtained here. Greater dimensions not only increase the structural safety, but simplify fabrication problems not considered within the scope of the present investigation.

However, as we shall see in the next section, heat transfer and material temperature limits impose an upper limit magnitude on R and δ and on the design feasibility consistent with the weight restriction $W_s + W_c \lesssim W_p$.

6. SIMPLIFIED HEAT TRANSFER

The most severe heat load conditions during entry occur, in general, along the leading edge of the canopy and the windward element of the shroud lines. The heat flux in these critical locations may be due either to free molecule flow (fm) regime at extreme altitude, transitional regime (tr) at intermediate altitudes, or stagnation flow heat transfer associated with boundary layer flow (bl) in the continuum regime of the lower altitudes.

6.1 Transitional Flow

The various regimes of interest are determined here by assuming that transition obtains when the density-dependent mean molecular free path $\lambda(\rho)$ becomes comparable with the dimension R of leading edge or shroud radii. In particular we assume that the density range of the transitional regime extends over a decade of mean free paths as defined by

$$\frac{1}{\sqrt{10}} \leq \frac{\lambda(\rho)}{R} \leq \sqrt{10} \tag{6.1}$$

with mid-transition density $\rho = \rho_{tr}$ obtained at $\lambda = R$.

In view of the inverse dependence of λ upon the local density $\rho(z)$ we determine from Eq. (6.1) the relation between mid-transition density $\rho = \rho_{tr}$ and the system dimension of interest R , utilizing standard air data at the earth's surface (Ref. 1),

$$\rho_o = 2.38 \times 10^{-3} \text{ slugs/ft}^3 \qquad \lambda_o = 2.18 \times 10^{-7} \text{ ft} \tag{6.2}$$

which yield

$$\rho_{tr} = \rho_o \lambda_o \cdot R^{-1} = 5.19 \times 10^{-10} R^{-1} \qquad (6.3)$$

Accordingly, the densities which define the limits of free molecule and continuum flows, in view of Eq. (6.1) are related to R by

$$\begin{aligned} &\text{free-molecule} && \rho \leq \rho_{fm} = 1.63 \times 10^{-10} R^{-1} \\ &\text{continuum} && \rho \geq \rho_{bl} = 1.63 \times 10^{-9} R^{-1} \end{aligned} \qquad (6.4)$$

Logarithmic plots of the limiting densities ρ_{tr}, ρ_{fm}, ρ_{bl} versus R are shown in Fig. 5. The reciprocal density is plotted as ordinate in Fig. 5 so that for exponential atmospheres of the type given by Eq. (4.1) the altitude increases in proportion to the ordinate, as indicated in the figure. Numerical data for the VM-3 and VM-7 atmospheres implies that over the range of "fine" characteristic dimensions $10^{-1} \geq R \geq 10^{-4}$ ft, transition may occur from 400 kft down to 150 kft as R is made smaller.

6.2 Free Molecule Heat Transfer

For densities $\rho < \rho_{fm}$ the convective heat transfer is calculated from the expression

$$Q_{fm}(\rho) = \frac{\rho V^3 (\rho)}{2J} \qquad (6.5)$$

corresponding to diffuse reflection of the free molecule flow incident perpendicularly upon a surface having an accommodation factor of unity (Ref. 6, p. 43). For the exponential atmosphere, the maximum free molecule heat flux $Q_{fm,max}$ is obtained by differentiation with respect to density

$$\frac{dQ_{fm}}{d\rho} = 0 \equiv \frac{d}{d\rho} \log Q_{fm} = \rho^{-1} - 3 c_e \qquad (6.6)$$

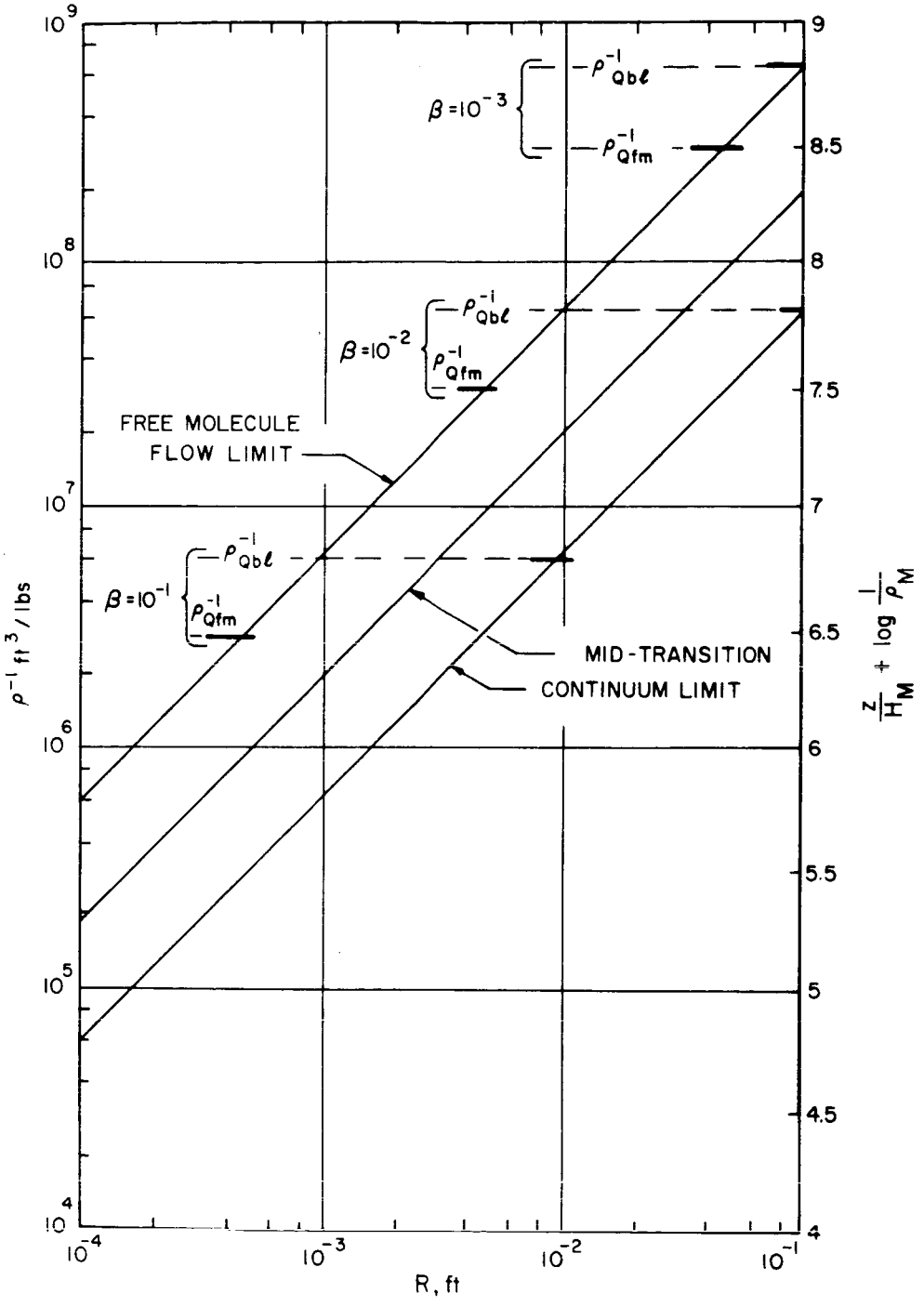

Figure 5

Variation of transition altitude with characteristic dimension R

PA-3-10526

which is satisfied at the density

$$\rho = \frac{1}{3c_e} \equiv \rho_{Q,fm} = \frac{2\beta \sin \gamma_e}{3 H_M} \tag{6.7}$$

or altitude

$$z = z_{Q,fm} = H_M \log \frac{3 H_M \rho_M}{2\beta \sin \gamma_e} \tag{6.8}$$

where substitution has been made for c_e from Eq. (4.4).

The variation of $\rho_{Q,fm}$ with β obtained from Eq. (6.7) is also shown in Fig. 5. The applicability of the associated expression for the maximum heat transfer

$$Q_{fm,max} = \frac{V_e^3 \beta \sin \gamma_e}{3 e H_M J} \tag{6.9}$$

is restricted to design dimensions R for which $\rho_{fm}(R) > \rho_{Q,fm}(\beta)$. This restriction is satisfied by the smaller values of $\beta \rightarrow 10^{-3}$ even for relatively large value of R, as shown in Fig. 5. Furthermore, it is seen that even for the largest value of $\beta = 10^{-1}$ the maximum value of R permissible in order to assure free molecule conditions at peak heating is achieved at $R \simeq 5 \times 10^{-4}$ ft, which is appreciably greater than the minimum required to satisfy the stress as given by Eqs. (5.8, 5.14).

6.3 Continuum Heat Transfer

For densities $\rho > \rho_{bl}$ the convective heat transfer is calculated from an expression applicable to high-speed stagnation flow (Ref. 1, pp. 96-97) normal to a "cold" cylindrical body of sectional radius R

$$Q_{bl} = \frac{645}{\sqrt{R}} \left(\frac{V}{10^4}\right)^{3.15} \left(\frac{\rho}{\rho_o}\right)^{0.50} \tag{6.10}$$

In the form given here the temperature-dependent properties have been accounted for by the numerical factor 645 consistent with the units V ft/sec, R ft and Q_{bl} BTU/ft^{2}sec . We note that, in contrast with the referenced heat flux formula, the stagnation enthalpy at the wall has been assumed negligible compared with the high-speed free-stream stagnation enthalpy. Furthermore, the numerical factor 645 appropriate for a cylinder, rather than 865 appropriate for a sphere, has been introduced here, consistent with the so-called Mangler transformation (Ref. 7) which interrelates the boundary layer effects in the two geometric configurations.

By substitution of density and trajectory relations into Eq. (6.10) and differentiation with respect to ρ

$$\frac{dQ_{bl}}{d\rho} = 0 = \frac{d}{d\rho} \log Q_{bl} = \frac{\rho^{-1}}{2} - 3.15\, c_e \tag{6.11}$$

we obtain the maximum heat flux

$$Q_{bl,\,max} = \frac{645}{\sqrt{R}} \left(\frac{V_e}{10^4}\right)^{3.15} \Big/ (6.3\, c_e\, e\, \rho_o)^{0.5} \tag{6.12}$$

at the density

$$\rho = \frac{1}{6.3\, c_e} \equiv \rho_{Q,\,bl} = \frac{\beta \sin \gamma_e}{3.15\, H_M} \tag{6.13}$$

which obtains at altitude

$$z = z_{Q,bl} = H_M \log \frac{6.3\, H_M \rho_M}{2\beta \sin \gamma_e} \tag{6.14}$$

We note that, in contrast with the result for $Q_{fm,max}$ in Eq. (6.9), the result for $Q_{bl,max}$ indicates an explicit dependence on the leading edge radius of curvature R. Furthermore, $\rho_{Q,bl}$ is formally smaller than $\rho_{Q,fm}$ and therefore $z_{Q,bl}$ is formally greater than $z_{Q,fm}$ in accordance with

$$z_{Q,bl} = z_{Q,fm} + H_M \log 2.1 \tag{6.15}$$

The dependence of $\rho_{Q,bl}$ and $z_{Q,bl}$ on β is also indicated in Fig. 5. The fact that $\rho_{Q,bl}$ occurs at higher altitudes than $\rho_{Q,fm}$ implies that if R is made sufficiently small to assure peak heating before transition to continuum, the subsequent continuum heat transfer will remain well below the peak value described by Eq. (6.12).

6.4 Transitional Heat Transfer

Regarding the transitional regime, no formulas are available at present for the heat flux Q_{tr}. However, as noted in Ref. 6, p. 59, because of the continuous behavior of heat transfer on decreasing Reynolds number in going from the boundary layer flow to the free molecule flow, the results for Q_{tr} in engineering practice may be interpolated between those of Q_{bl} and Q_{fm}. We show in the following paragraph that the ratio Q_{fm}/Q_{bl} is of the order of unity throughout the transitional regime, and utilize this fact in postulating an interpolation formula for the transitional heat flux Q_{tr}.

The ratio Q_{fm}/Q_{bl} obtained from Eqs. (6.5) and (6.10) is

$$\frac{Q_{fm}}{Q_{bl}}(\rho) = \frac{10^{12}\sqrt{\rho\ \rho_o\ R}}{1290\ J\left(V/10^4\right)^{0.15}} \qquad (6.16)$$

At the mid-transition density $\rho = \rho_{tr}$ given by Eq. (6.3) we have in the approximation that $\exp .15\, c_e\, \rho_{tr} \simeq 1$

$$\left(\frac{Q_{fm}}{Q_{bl}}\right)_{\rho=\rho_{tr}} = \frac{10^{12}\ \rho_o\sqrt{\lambda_o}}{1290\ J\left(V_e/10^4\right)^{0.15}} \qquad (6.17)$$

an expression independent of R.

Numerical substitutions with a representative entry speed $V_e = 10^4$ ft/sec yield:

$$\frac{Q_{fm}}{Q_{bl}} \simeq 1.10 \qquad \text{at} \qquad \rho = \rho_{tr}\ , \qquad V_e = 10^4\ \text{ft} \qquad (6.18)$$

Within the transitional regime defined in Eq. (6.4) the heat flux ratio for $V_e = 10^4$ ft/sec varies in the range

$$.62 = \frac{1.10}{10^{1/4}} < \frac{Q_{fm}}{Q_{bl}} < 1.10(10)^{1/4} = 1.97 \qquad (6.19)$$

Finally since the ratio in Eq. (6.17) is proportional to $V_e^{-0.15}$, the limits indicated in Eq. (6.19) may change as V_e ranges over the interval $6\text{x}10^3$ ft/sec $< V_e < 16\text{x}10^3$ ft/sec. The extreme limits of the Q_{fm}/Q_{bl} ratio are obtained by changing 1.96 to 2.12 as $V_e \rightarrow 6000$ ft/sec, and 0.62 to 0.58 as $V_e \rightarrow 16,000$ ft/sec.

Based on the limited variation of the ratio Q_{fm}/Q_{bl} through the transitional regime, we employ, where necessary, an interpolation formula for calculating Q_{tr} as described below with the aid of Fig. 6. We consider the entry system with given β and leading edge dimension R. The given β determines the $\rho^{-1}_{Q,fm}$ and $\rho^{-1}_{Q,bl}$ lines introduced in the figure. These lines intersect the lines representing the transition density limits as shown in the figure, with point A at the intersection of ρ_{fm} and $\rho_{Q,fm}$, and point B at the intersection of ρ_{bl} and $\rho_{Q,bl}$. The radii R at which A and B are obtained is designated by R_A, R_B. Now if the given R is greater than R_B, then transition precedes the peak heat flux (at density $\rho_{Q,bl}$) and the magnitude of this heat transfer is determined unambiguously as $Q_{bl,max} = Q_{bl,max}(\beta, R)$ given by Eq. (6.12). Similarly, if R is less than R_A the peak heat flux is obtained before transition at the density $\rho_{Q,fm}$ at the peak value $Q_{fm,max} = Q_{fm,max}(\beta)$ given by Eq. (6.7). If the given R is between R_A and R_B we employ the following interpolation to calculate the transitional peak heat flux

$$Q_{tr,max} = \frac{\left(\log \frac{R}{R_A}\right) Q_{bl,max}(\beta, R) + \left(\log \frac{R_B}{R}\right) Q_{fm,max}(\beta)}{\log \frac{R_B}{R_A}} \qquad (6.20)$$

This interpolation form is constructed so as to satisfy the dominant regimes approached as $R \to R_A$, $Q_{tr} \to Q_{fm}$ and $R \to R_B$, $Q_{tr} \to Q_{bl}$. Furthermore, the use of a logarithm rather than linear interpolation in R suppresses the relative importance of this parameter, consistent with its role in the logarithmic plots of Fig. 5.

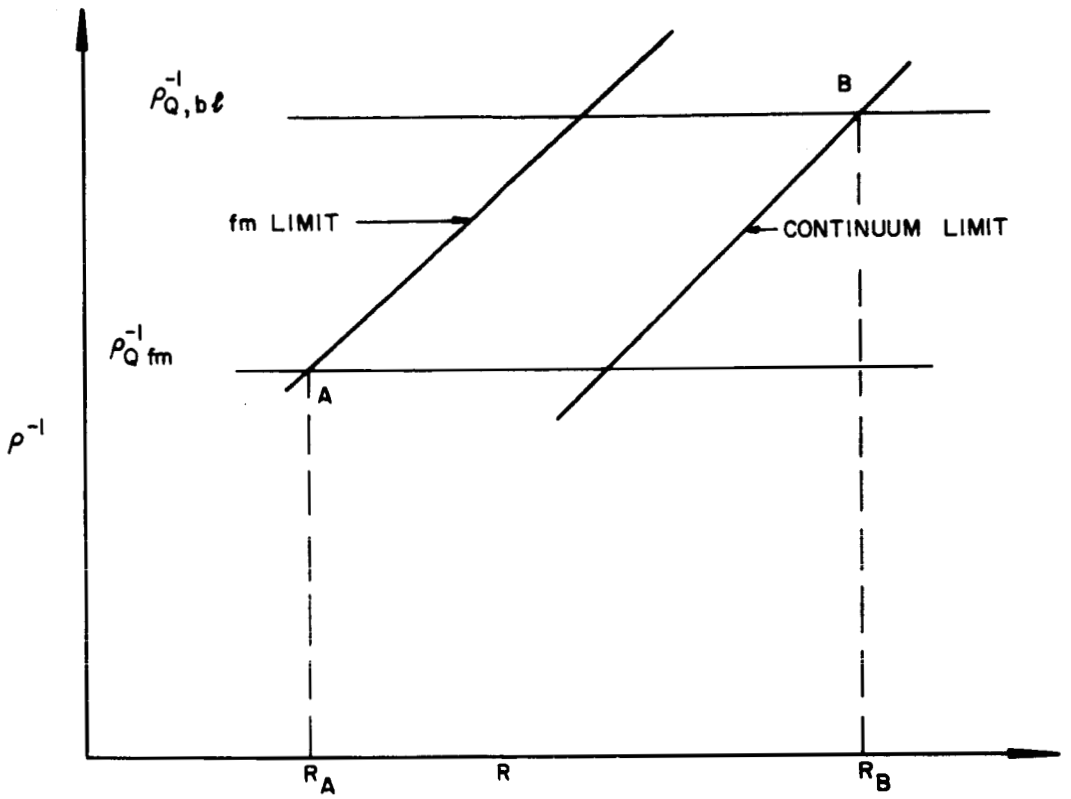

Figure 6

Sketch of interpolation zone for postulated transition heat flux formula Eq. 6.20. Interpolation required if, for specified R and β, the characteristic dimension R is intermediate between R_A [obtained from $\rho_{fm}(\beta) = \rho_{Q,fm}(R_A)$] and R_B [obtained from $\rho_{bl}(\beta) = \rho_{Q,bl}(R_B)$].

PA-3-10527

7. FEASIBILITY LIMITS

As we have shown in Section 5, if the tensile strength of the chute material is of the order of 50,000 to 100,000 psi, then the structural weight requirements $(W_c + W_s)$ for supporting the maximum deceleration loads are small compared with the payload weight W_p. However, the temperature dependence of tensile strength imposes a limit on the allowed material temperature, which must therefore remain below a specified maximum value T_{max} during entry. We therefore consider the feasibility limits which relate the allowed temperature T_{max} to entry heating. In particular we determine the relation between T_{max} and the entry velocity V_e which, as shown in Section 6, governs the maximum heat loads imposed on the vulnerable elements of the chute design; i.e., on the leading edge of the canopy and on the windward elements of the shroud lines. Thus we determine the feasibility limits for two essentially different deceleration system designs. The first of these, having "fine" characteristic dimension R (canopy leading edge radius or shroud line radius) will experience maximum heat transfer in the free molecule flow of high-altitude regime, so that when continuum flow is established at the lower altitude, convection heating is well below its possible peak magnitude. In this system the relation between T_{max} and V_e is found to be independent of the (small) deceleration system weight. The second system envisages "blunt" dimensions R which incur transitional and/or continuum flow heat transfer at peak magnitude. Because this peak magnitude depends inversely on $R^{1/2}$, it can be mitigated only by increasing R, and therefore, by increasing the deceleration system weight. Thus the relation determined between T_{max} and V_e for the "blunt" design depends significantly on the deceleration system weight. It is found then that a dominant system parameter which appears in the feasibility limit relation connecting T_{max} and V_e is the weight of the "torus" forming the "blunted" leading edge of the canopy.

7.1 Feasibility Limits with Maximum Heating $Q_{fm,max}$

7.1.1 Stress Constraints

It is seen from Fig. 5 that even with the largest value $\beta = 10^{-1}$, the peak heating will occur in the free molecule flow regime, provided the "fine" dimension R does not exceed an upper limit $R_{max} = 5x10^{-4}$ ft. Lower limits on these dimensions arise from strength requirements as expressed by Eqs. (5.8, 5.14) for Nomex parachutes under the most severe entry conditions under consideration. Therefore the feasible design dimension by which peak heat transfer is incurred in the free molecule flow regime is constrained in the first place by the restriction

$$2x5x10^{-4} \text{ ft} \geq \delta \geq \delta_{min} = 1.4x10^{-5} \text{ ft} \tag{7.1}$$

$$5x10^{-4} \text{ ft} \geq R_s \geq \sqrt{\frac{1.9x10^{-5}}{N_s}} \tag{7.2}$$

valid for all $\beta \leq 10^{-1}$ and $V_e \leq 16$ kft/sec.

As an example of satisfactory design data from the stress viewpoint for $\beta = 10^{-3}$ we may select $\delta = .001$ in; $R_s = .0036$ in for $N_s = 300$. The dimension D is, then, D = 76.5 ft. The corresponding canopy weight $W_c = 23.3$ lb and shroud weight $W_s = .6$ lb total less than the maximum permissible chute weight of 50 lb. These results hold for Nomex with $\sigma \simeq 50,000$ psi and density $\rho_c = 86.3$ lb/ft^3.

It is to be noted that the stress conditions for metals of greater tensile strength have smaller lower limits than those for Nomex in Eqs. (7.1) and (7.2), so that despite the greater metallic densities, the strength requirements can be achieved with $W_c + W_s << W_p$. Furthermore, the high temperature strength of metals enables extension of feasibility limits with increasing entry velocity beyond those determined below for Nomex.

7.1.2 Temperature Constraints

Next we estimate the entry velocity limitation arising from peak heat loads. We rewrite Eq. (6.7) in the form

$$Q_{fm,\,max} = \frac{\beta\, V_e^3 \sin \gamma_e}{3\, e\, H_M\, J} \tag{7.3}$$

and consider its effect on the canopy leading edge and on the shroud lines.

In applying $Q_{fm,\,max}$ to the leading edge we consider that, because of the effective bluntness $\delta/2$ of this element, the mean heat load is $\frac{1}{2} Q_{fm,\,max}\, \pi D (\pi \frac{\delta}{2})$. The averaging performed here allows for the inclination of the blunted leading edge surface elements to the direction of the incident flow. Gray-body re-radiation from the surfaces affected by the incident flow is given by $\sigma' \epsilon\, T^4\, \pi\, D\, (\pi \frac{\delta}{2})$ where T has been assumed uniform throughout the leading edge cross section by virtue of its small dimensions and good thermal conductivity. Therefore under the assumption of quasi-equilibrium between mean heat influx and gray-body re-radiation, we obtain the following equation for the maximum temperature T_{max} in the leading edge

$$\sigma' \epsilon\, T_{max}^4 = \frac{1}{2}\, Q_{fm,\,max} \tag{7.4}$$

Analogous considerations applied to the shroud lines indicate

$$\sigma' \epsilon\, T_{max}^4 = \frac{1}{4}\, Q_{fm,\,max} \cos^2 60 \tag{7.5}$$

Therefore the higher temperature calculated from these equations, i.e., that given by Eq. (7.4) for the leading edge, governs the feasibility limit in free molecule flow.

Substituting from Eq. (7.4) into Eq. (7.3) we have, upon simplifying, the following relation between T_{max} and V_e:

$$T_{max} = \left(\frac{\beta \sin \gamma_e}{6 \sigma' \epsilon e H_M J} \right)^{1/4} V_e^{3/4} \qquad (7.6)$$

Substitution of numerical values

$\sigma' = .476 \times 10^{-12}$ BTU/ft^{2}sec (deg R)^4 $\qquad$ J = 778 ft-lb/BTU

$\sin \gamma_e = .259$ $\qquad$ e = 2.72 $\qquad$ $H_M = 50.5 \times 10^3$ ft

results in

$$\epsilon^{1/4} T_{max} = 5.37 \beta^{1/4} V_e^{3/4} \qquad (7.6')$$

Curves of T_{max} versus V_e obtained from Eq. (7.6') for several values of β are shown in Fig. 7. A tabulation of maximum entry velocities versus β for Nomex with $T_{max} = 500^{\circ}F$ with assumed value of $\epsilon = .92$

Table of $V_{e,max}$ for Nomex

β slugs/ft^2	10^{-1}	10^{-2}	10^{-3}
$V_{e,max}$ ft/sec	2090	4510	9700

The minimum value of the chute weight for the $\beta = 10^{-3}$ design, obtainable from Eqs. (5.8, 5.11) is

$$W_{c,min} + W_{s,min} = 0.27 + 0.46 = 0.73 \text{ lb} \qquad (7.7)$$

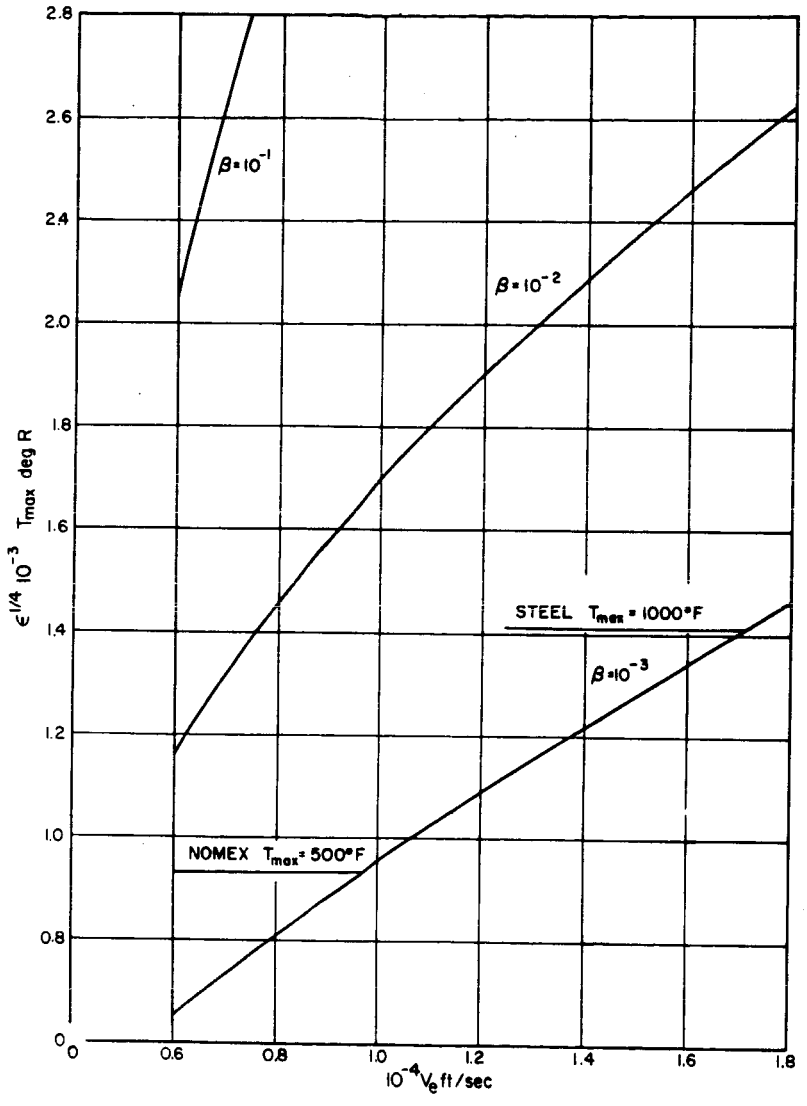

Figure 7

Feasibility limit curves for entry heat pulse in free molecule flow

PA-3-10528

7.2 Feasibility Limit with Maximum Heating $Q_{bl,\,max}$

As noted above the required deceleration system weight is now dependent on preventing excessive temperature in the blunted leading edge of the canopy. The "blunting" of the shroud lines need not incur much additional weight, since the shroud lines are favorably inclined to the direction of flow [Cf. Eqs. (7.4, 7.5) for the effect of inclination].

Accordingly, we introduce the parameter representing the weight of the deceleration system, as consisting essentially of the ring weight:

$$\mu = W_r / W_p \tag{7.8}$$

in terms of which we may conveniently express other design dimensions, such as diameter D, and the ring radius R_r:

$$D = \sqrt{\frac{8\, W_p\, (1+\mu)}{\pi\, g_E\, \beta}} \tag{7.9}$$

$$R_r = \frac{1}{\pi}\sqrt{\frac{\mu\, W_p}{\rho_r\, D}} = \frac{1}{\pi}\left(\frac{\pi}{8}\right)^{1/4}\sqrt{\frac{\mu}{\rho_r}}\left(\frac{g_E\, \beta\, W_p}{1+\mu}\right)^{1/4} \tag{7.10}$$

The latter dimension is of dominant importance in the maximum stagnation heat flux Eq. (6.12).

We now calculate the maximum temperature with quasi-equilibrium between continuum heat in flux and thermal re-radiation [Cf. Eq. (7.4)]

$$\sigma' \epsilon\, T_{max}^4 = \frac{1}{4}\, Q_{bl,\,max} = \frac{161}{\sqrt{R_r}}\left(\frac{V_e}{10^4}\right)^{3.15}\left(\frac{\rho_{Q,\,bl}}{e\rho_o}\right)^{1/2} \tag{7.11}$$

where Eqs. (6.12, 6.13) have been used and allowance has been made for re-radiation along the whole cross sectional circumference of the ring. Further, we may express the latter equation in the form

$$\sigma' \epsilon \, T_{max}^4 = F(\beta, \mu) \, V_e^{3.15} \tag{7.12}$$

where F is a function of the system design parameters β , μ .

$$F(\beta, \mu) = \frac{161}{10^{12.6}} \left(\frac{8}{\pi}\right)^{1/8} \frac{\sqrt{\pi}}{\sigma'} \left(\frac{\rho_r^2}{g_E W_p}\right)^{1/8} \left(\frac{\sin \gamma_e}{3.15 \, e \, H_M \, \rho_o}\right)^{1/2} \left(\frac{1+\mu}{\mu^2}\right)^{1/8} \beta^{3/8} \tag{7.13}$$

Therefore, the feasibility limit equation, Eq. (7.12), rewritten in the form

$$\epsilon^{1/4} \, T_{max} = F^{1/4} \, V_e^{0.7875} \tag{7.14}$$

implies a weak dependence of T_{max} on μ implicit in $F^{1/4}$.

Limit curves calculated from Eq. (7.14) for Nomex density $\rho_r = 86.3$ lb/ft^3 are shown in Fig. 8 for several values of μ and β . Continuum conditions are satisfied if $R_r > \sqrt{10} \, \lambda(\rho)$ which, by use of Eq. (7.10), may be converted to an expression relating β and μ

$$\beta > \left(\frac{10 \, \lambda_o \, \rho_o \, e \, H_M}{\sin \gamma_e}\right)^{4/5} \left(\frac{\rho_r^2}{g_E W_p}\right)^{1/5} \left(\frac{1+\mu}{\mu^2}\right)^{1/5} \tag{7.15}$$

The special form of Eqs. (7.14) and (7.15) with Nomex data under the entry conditions of interest is

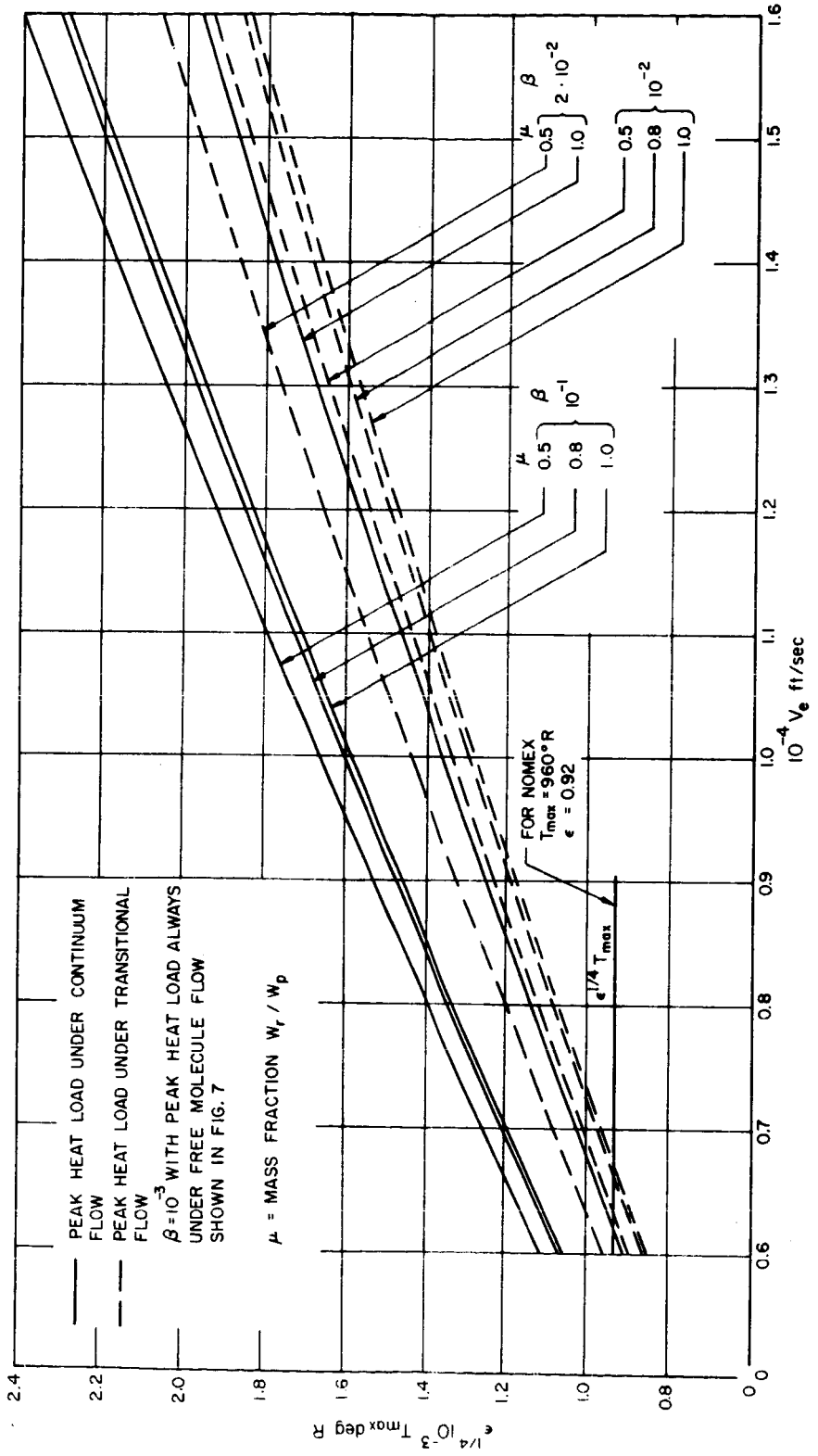

Figure 8
Feasibility limit curves for entry heat pulse in continuum and transition flow

PA-3-10529

$$\epsilon^{1/4} T_{max} = 1.36\left(\frac{1+\mu}{\mu^2}\right)^{1/32} \beta^{3/32} V^{0.7875} \qquad (7.14')$$

$$\beta > 1.67\text{x}10^{-2}\left(\frac{1+\mu}{\mu^2}\right)^{1/5} \qquad (7.15')$$

From these expressions we obtain the limit curves showing as solid curves the variation of $\epsilon^{1/4} T_{max}$ versus V_e in Fig. 8. In the same figure, the transitional flow limits are shown in dashed curves. We note that subject to the restriction of the weight parameter $\mu \leq 1$ continuum can be obtained, in view of Eq. (7.15'), only if $\beta > 1.9 \times 10^{-2}$ slugs/ft^2 . Thus, the results in Fig. 8 show the $\beta = 10^{-1}$ family in continuum flow for the indicated values of $\mu \leq 1$; the $\beta = 10^{-2}$ in transition flow of indicated values of $\mu \leq 1$. For $\beta = 2\text{x}10^{-2}$ continuum is obtained at $\mu = 1$, but for $\mu = .5$, transitional flow will obtain at maximum entry heating.

It is to be noted that the $\beta = 10^{-3}$ does not appear in Fig. 8, because for the Nomex system all possible configurations subject to $\mu \lesssim 1$ will experience peak heat load in free molecule flow. Thus, the maximum β of interest in the boundary layer regime is about $2\text{x}10^{-2}$. Accordingly, as shown in Fig. 8, the maximum feasible entry velocity in "laminar" peak heating is 6330 ft/sec.

Finally, we note from Figs. 7 and 8 that if entry at small speeds V_e is to be achieved with the higher β system ($\beta \rightarrow 10^{-1}$) the blunted design, rather than the fm design, becomes feasible, but for high-speed entry the fm design with $\beta \rightarrow 10^{-3}$ governs the feasibility limit.

8. DISCUSSION OF RESULTS

The feasibility limit of high-speed entry with all-Nomex parachutes is obtained from the curves in Figs. 7 and 8 by locating the value of V_e at the ordinate

$$\epsilon^{1/4} T_{max} \cong (.92)^{1/4} (460 + 500) = 940^{\circ}R$$

The value of $\epsilon \simeq 0.92$ used here is presumably obtainable* by appropriate coating or processing of Nomex. It is thus seen that to achieve high entry velocities with Nomex, it is necessary to have the lowest possible ballistic coefficient $\beta \simeq 10^{-3}$, with "sharp" leading edges (windward elements) which experience peak heat load in the free molecule regime. The feasible entry velocity from Fig. 7 is then $V_e \simeq 9,700$ ft/sec, well above the feasible maximum value obtained from Fig. 8 in laminar (continuum) heat transfer $V_e \simeq 6,730$ ft/sec, $\beta = 2 \times 10^{-2}$. In the latter (bl) design, the parachute weight is 50 lbs ($\mu = 1$), incurred mostly in the weight of the toroidal "blunt" leading edge of the canopy. On the other hand, the former (fm) design requires a minimum weight of only [Cf. Eq. (7.7)]

$$W_{c,min} + W_{s,min} \simeq (0.27 + 0.46) = 0.73 \text{ lb} \qquad (8.1)$$

or $\mu = 0.015$. The weight and maximum velocity advantage of the fm versus the bl parachute design can be ascertained by comparing the temperature maxima obtainable under these flow conditions, using Eqs. (7.6', 7.14'):

---

* "Study of Expandable, Terminal Decelerators for Mars Atmosphere Entry," Goodyear Aerospace Corporation, Akron, Ohio, October 3, 1966

$$\frac{T_{max,\,fm}}{T_{max,\,bl}} = 3.95\left(\frac{\mu^2}{1+\mu}\right)^{3/32} \beta^{5/32}\, V_e^{-.0375} \qquad (8.2)$$

This ratio decreases as the chute weight associated with the mass parameter μ decreases, as β decreases, and as the entry velocity increases.

The relatively small minimal weights for the fm design with Nomex, $W_{c,\,min} + W_{s,\,min} << 50$ suggest the possibility of using denser, high-temperature high-strength metals for further extending the feasible entry velocity within the parachute weight restriction of 50 lb. Consider, for example, stainless steel (SS 301) which retains a tensile strength of about 60,000 psi at the high temperature of 1000°F. For this temperature we obtain from Fig. 7 the following table of feasible entry velocities

β	10^{-1}	10^{-2}	10^{-3}
V_e	3660	7890	17,000

To assure meeting both stress requirements and fm conditions at maximum heat transfer, it is sufficient to keep the same design dimensions as calculated above for Nomex. Accordingly, for example, for $\beta = 10^{-3}$ the minimal weight requirement obtained by scaling the result in Eq. (8.2) with the steel-to-Nomex density ratio of 5.7 is

$$W_{c,\,min} + W_{s,\,min} = 1.5 + 2.7 \qquad (8.3)$$

Implicit in the minimal weight $W_{c,\,min}$ is a minimal canopy thickness $\delta_{min} \simeq 1.4 \times 10^{-6}$ ft , in view of the scaling formula Eq. (5.7). From the fabrication viewpoint such a minimal thickness may indeed be

problematic. We note, however, that the canopy weight may be increased from its minimal value of 1.5 lb in Eq. (8.3) to 47.3 without exceeding the parachute weight restriction of 50 lb. With the indicated increase, the effective thickness δ will also increase to a practicable value of $\delta \simeq (47.3/1.5)\,\delta_{min} \simeq 4.4\text{x}10^{-5}$ ft = $5.3\text{x}10^{-4}$ in.

Finally, we note that the T_{max} as discussed in Section 6 generally occurs at a higher altitude (i.e., earlier) than the peak stress. Cooling in the interval between peak heat load and peak stress permits an increase in structural strength above that employed in the calculations. From this viewpoint the calculations are somewhat conservative. However, since T_{max} depends on the fourth root of the heat flux, inclusion of the strength recovery effect in the calculation does not appear warranted.

9. REMARKS ON SHOCK IMPINGEMENT

We consider the shock wave which may impinge on the parachute due to the bow shock formed by the primary body.

The primary body diameter D_p is assumed to be small compared with D (see Appendix)

$$D_p \simeq \sqrt{10^{-3}}\, D = .0316\, D \tag{9.1}$$

The profile of the (hypersonic) shock wave, formed at altitudes where $D_p \gg \lambda$, will be assumed in the approximate parabolic form, given by blast wave theory (Ref. 8)

$$\frac{y}{D_p} = 0.9\left(C_{D_p}\right)^{1/4}\left(\frac{x}{D_p}\right)^{1/2} \tag{9.2}$$

where

x = axial distance measured from nose

y = lateral (radial) distance from axis

$C_{D_p} \simeq 1$ = spherical nose drag coefficient

In the "exit" plane of the conical canopy the radius of the shock wave is

$$y' \approx 0.9\,(D_p\, D)^{1/2} = .16\, D << \frac{D'}{2} = \frac{D}{2\sqrt{2}} \tag{9.3}$$

Therefore the axisymmetric shock front will lie well within exit hole of the canopy, without giving rise to an impingement problem.

A portion of the shroud lines near their attachment to the primary body will in general be submerged under the bow shock wave developing at the lower altitudes, and in the "entropy layer" close to the body axis. From the geometry of the shock profile Eq. (9.2) impingement will occur as a "weak shock" at distance of radial distance of about D_p from the axis, and an axial distance of $3\ D_p$ downstream of the nose. Although the temperature is high in the wake of the shock and entropy layer, the density is in fact smaller than ambient density. Hence the fm design with its fine shroud lines may remain in free molecule flow well below the altitudes where the primary shock has developed, and its heating rate is not enhanced under these conditions. Analogous considerations indicate that the "blunt" design with fewer shroud lines will not experience more severe heating in the "weak shock" and entropy layer than due to that of the ambient flow. Finally to assure that the fine shroud lines of the fm design will not be submerged under the shock wave profile given by Eq. (9.2), they may be terminated on a few short "blunt" lines piercing the bow shock profiles and continuing the connection to the primary body. Details of such a composite attachment design would require further study.

10. CONCLUSIONS

The following conclusions are made on the basis of the present investigation.

1a. The axisymmetric Nomex parachute will survive laminar entry heating pulse up to an entry velocity $V_{e_1 max} = 6330$ ft/sec with a ballistic coefficient of $\beta = 2 \times 10^{-2}$ slugs/ft^2 corresponding to maximum deceleration system weight of 50 lb. Most of this system weight is due to the "blunt" toroidal ring at the leading edge of the canopy.

1b. With the weight restriction as above, an entry system designed to undergo entry heat pulse under free molecule flow conditions can survive entry heating up to entry velocities V_e as listed below for two feasible high-temperature materials.

Maximum V_e with Heating Pulse in Free Molecule Flow

β slugs/ft^2	10^{-1}	10^{-2}	10^{-3}
V_e ft/sec (Nomex at 500°F)	2090	4510	9700
V_e ft/sec (Steel at 1000°F)	3660	7890	17,000

2. With the weight and entry velocity restrictions as above, the heated parachute can survive the peak dynamic loads arising in all flow regimes considered.

3. The Mars atmosphere entry conditions are favorable to the possible utilization of "sharp" leading edge deceleration systems which enable critical entry heating in the

free molecule flow regime. As a consequence, all-metal deceleration systems, possessing strength at high temperature, provide an approach to the extension of entry velocity limits, without incurring excessive weight penalties.

11. ACKNOWLEDGMENTS

The writer is pleased to acknowledge helpful discussions with E. Laumann and B. Dayman of JPL and with G. Bergman and J. Grzesik of NESCO.

12. REFERENCES

1. Martin, J. J., Atmospheric Reentry, Prentice-Hall, Inc., Englewood Cliffs, N. J., (1966).

2. Loh, W. H. T., "Ballistic Reentry at Small Angles of Inclination," J. American Rocket Society, Vol. 32, (1962), p. 718.

3. Gazley, C., Jr., "Heat Transfer Aspects of the Atmospheric Reentry of Long Range Ballistic Missiles," Report R-273 (Santa Monica, California: The RAND Corporation, August 1, 1954).

4. E. I. Du Pont de Nemours Co. - Bulletin N-201, "Properties of Nomex," October 1966.

5. E. I. Du Pont de Nemours Co. - Bulletin D-173, "The Tenacity and Elongation of Dacron," January 1964.

6. Probstein, R. F., "Heat Transfer in Rarefied Gas Flow," Theory and Fundamental Research in Heat Transfer, The MacMillan Company, (1963), Ed. J. A. Clark.

7. Schlichting, H., Boundary Layer Theory, McGraw-Hill Book Co., Inc., New York, (1960), p. 190.

8. Lykoudis, P. S., "Ionization Trails," Proceedings of the 1961 Heat Transfer and Fluid Mechanics Institute, Stanford University Press, Stanford, California, (1961).

PRECEDING PAGE BLANK NOT FILMED.

APPENDIX

PRECEDING PAGE BLANK NOT FILMED.

Exhibit No. 1
RFQ BE-38465
21 March 1967

A STUDY OF THE USE OF A PARACHUTE ENTRY SYSTEM FOR MARS LANDER

Introduction

The relatively tenuous atmospheric conditions expected to exist at Mars present a significant engineering challenge in determining the optimum design for a small survival scientific entry probe. Studies have been conducted of blunt body aerodynamic decelerators, single and multistage subsonic and supersonic parachutes, guided retro rocket landing systems and lifting entry. Each of these systems have certain drawbacks.

An alternate entry system has been proposed; i.e., a payload suspended from a large diameter ring parachute which was opened outside the sensible atmosphere of Mars. This system could conceivably have a lower impact velocity than the blunt body devices, not require the Mach and/or altitude sensors required for parachutes and would avoid the opening shock problems and would not require the altitude and directional control systems required for retro and lifting entry. On the other hand several significant questions can be raised concerning the feasibility of such a system. Two questions in particular require answers before any detailed feasibility study can be considered.

The two questions requiring answers are:

1. Assuming state-of-the-art materials are used, can a parachute survive the entry heating pulse?

2. Can this heated parachute survive the peak dynamic pressure pulse while carrying a meaningful payload?

A first order study shall be made to answer these two questions.

Assumptions

Certain assumptions must be made in order to limit the scope of the study. A number of basic assumptions* are listed below.

1. Parachute configurations

   a. Conical, flat annular with central open area equal to 1/2 overall frontal area (A_o)

   b. Shroud line length equal to chute maximum diameter

*Some of these assumptions are arbitrary. If it is shown that any of them are unnecessarily restrictive or avoidable, they may be changed upon request.

c. $C_D = 1/2$ (based upon overall frontal area)

d. Weight may not exceed weight of payload

2. Payload configuration

a. Hemisphere-cylinder with frontal area $(A_p) = .001\ A_o$

b. Payload weight of 50 lbs.

3. Loads

a. Equal distribution over canopy

b. Uniform shroud line loading

c. Parachute opening shock $\ll q_{max}$ loading

4. Heating

a. Critical peak heating is laminar, convective to cylindrical chute leading edge or to shroud line at chute attachment point

b. Heating on rest of chute is not critical but assume that chute panel temperatures of 250°F exist at q_{max}

c. Radiation is outward from grey body to black space

5. Materials

a. Payload container made of non-ablative material

b. Chute and shroud lines of Dacron and Nomex

c. Do not be concerned about minimum gages of materials

Study Parameters

The effects of variation of several mission parameters should be investigated in the study. These are:

1. Ballistic coefficients (slugs/ft^2) between 0.001 and 0.10

2. Trajectory angle at 800,000 ft is -15° only

3. Velocity at 800,000 ft between 6,000 and 16,000 ft/sec

4. Mars atmosphere described by VM-3 and VM-7 engineering models

Technical Resources Available

The JPL will support this study by making available trajectory calculations which describe the dynamic pressure and the ideal gas stagnation point heating rate histories. Various other information can be made available such as prior parachute and drogue studies and characteristics of fabrics at elevated temperatures.

Study Results

1. Describe the assumptions that were required.

2. Determine under what parametric combinations that the mission is feasible.

3. For feasible missions describe (giving estimates of the certainty tolerance):

   a. Parachute weight and material

   b. Leading edge diameters

   c. Shroud line sizes

   d. Critical temperature histories

   e. Other unique characteristics

4. Recommend alternate considerations which could lead to further study.

Presentation of Results

Intermediate oral presentations shall be made at JPL after two weeks and four weeks of effort to describe progress and plans to date. At the completion of the study, both an oral presentation and a memorandum final report will be due at JPL.

2-15-67